An approach to reduce the antiferromagnetic coupling of antiphase boundaries in half-metallic magnetite films

P. Li, W. Y. Cui, and H. L. Bai

Citation: J. Appl. Phys. **114**, 213902 (2013); doi: 10.1063/1.4837658
View online: http://dx.doi.org/10.1063/1.4837658
View Table of Contents: http://jap.aip.org/resource/1/JAPIAU/v114/i21
Published by the AIP Publishing LLC.

An approach to reduce the antiferromagnetic coupling of antiphase boundaries in half-metallic magnetite films

P. Li, W. Y. Cui, and H. L. Bai[a)]
Tianjin Key Laboratory of Low Dimensional Materials Physics and Preparing Technology, Institute of Advanced Materials Physics, Faculty of Science, Tianjin University, Tianjin 300072, People's Republic of China

(Received 2 September 2013; accepted 14 November 2013; published online 3 December 2013)

Highly conductive ($\sim 10^5\ \mu\Omega$ cm) Mn doped epitaxial Fe_3O_4 films were fabricated by reactive sputtering. The larger size of magnetic domains compared to grain size with the increasing Mn content indicates that the partial antiferromagnetic coupling across the antiphase boundaries has been weakened, which was further demonstrated by the smaller exchange bias, faster saturated magnetization, and decreasing exchange interaction J_{AF}. The decrease of antiferromagnetic strength originates from the larger Mn-O bond length than that of Fe-O bond. The first-principle calculation shows that the half-metallic feature (100% spin polarization) of Fe_3O_4 was unchanged with the incorporation of Mn atoms. © *2013 AIP Publishing LLC*. [http://dx.doi.org/10.1063/1.4837658]

I. INTRODUCTION

Magnetite is a mixed-valence inverse spinel with Fe^{3+} occupied tetrahedral (A) sites and Fe^{2+} and Fe^{3+} alternative occupied octahedral (B) sites for the temperature below Verwey transition ($\sim$124 K).[1] Fe_3O_4 is always pursued in spintronics due to its high Curie temperature ($\sim$858 K) and unique band structure with $t_{2g\downarrow}$ located in Fermi level.[2] Nevertheless, the application of Fe_3O_4 films in spintronics was restricted due to the relative low spin injection efficiency from Fe_3O_4 into semiconduction[3,4] and rather small magnetoresistance in Fe_3O_4-based magnetic tunneling junction[5,6] (MTJ). These are thought to be caused by the natural growth defects, antiphase boundaries (APBs), which are the coalescence of independent nucleated crystallographic domains. Attributed to the relative lower crystal symmetry of inverse spinel, APBs were usually observed in the epitaxial Fe_3O_4 films deposited on MgO, $SrTiO_3$, c-Al_2O_3 and $MgAl_2O_4$, etc.[7–14] The cation sublattice (Fe) shifts 1/4a along[110] or 1/2a along[100] with the face-centered anion sublattice (O) undistorted. According to Sawatzky,[15] the exchange integral J across the boundaries is proportional to $\cos^2\theta$, where θ is the bond angle of cation–anion–cation. The bond angles of Fe–O–Fe across APBs in epitaxial Fe_3O_4 films are nearly $\sim$180°, where the strong antiferromagnetic couplings forms.[16] This antiferromagnetic coupling across APBs has a great impact on the magnetic and transport properties of epitaxial Fe_3O_4 films, for instance, the unsaturated magnetization and linear magnetoresistance at high fields.[16,17] The presence of antiferromagnetic coupled APBs decreases the spin polarization near the Fermi level,[18] the corresponding spin injection efficiency, and MR ratio in MTJ.[6] Therefore, searching for an approach to decrease the antiferromagnetic coupling strength across APBs is of vital importance for the applications of half-metallic Fe_3O_4 films. Although buffer layers, for instance Fe, Cr, and TiN[19,20] can decrease the density of APBs, the coupling strength and bond angles of cation–anion–cation across APBs are nearly unchanged during the epitaxial growth. Hence, substituting iron atoms near APBs by other 3d metals to modify the antiferromagnetic coupling strength is another possible solution to this problem. Given that the insulating feature of $NiFe_2O_4$ and $CoFe_2O_4$ and antiferromagnetic characteristic of $ZnFe_2O_4$, manganese with larger ionic radius than iron is selected to reduce the antiferromagnetic coupling of cation–anion–cation across APBs and maintain the half-metallic band structure.

In this work, we found that the antiferromagnetic coupling (Fe-O-Fe) across the natural growth defect APBs in epitaxial Fe_3O_4 thin films could be reduced by Mn doping (smaller J_{AF} for Mn-O-Fe or Mn-O-Mn than that for Fe-O-Fe). Meanwhile, the half metallic band structure near the Fermi level remains unchanged as indicated by the first-principal calculations.

II. EXPERIMENTAL DETAILS

The epitaxial $Mn_xFe_{3-x}O_4$ films were fabricated by reactive sputtering facing Fe targets in the atmosphere of Ar and O_2 on MgO (001) substrates. The thickness of the films was determined to be $\sim$150 nm with a Dektak 6 M surface profiler. The content x was controlled by the number of pure manganese pieces on Fe targets. The manganese contents ranging from $x = 0.12$ to 0.65 were confirmed by energy-dispersive X-ray spectroscopy, and the crystal structure was characterized with X-ray diffraction (XRD, Cu Kα source, $\lambda = 1.5406$ Å), including normal θ-2θ scans and φ scans. The surface morphology and magnetic domains were directly investigated with magnetic force microscopy (MFM). The magnetic properties were carried out with a Quantum Design magnetic property measurement system. The transport properties were measured in standard four probe method with a physical property measurement system. The density of states and exchange integral of cation-oxygen-cation in the Mn doped Fe_3O_4 were calculated by VASP code and generalized gradient approximation (GGA) of Perdew Burk Erezerhof (PBE) with DFT+U technique.

a)Author to whom all correspondence should be addressed. E-mail: baihaili@tju.edu.cn

III. RESULTS AND DISCUSSION

Figure 1(a) gives the XRD θ-2θ patterns of the Mn doped Fe_3O_4 films on MgO (001). All the films with different Mn contents are (00l) orientation out of plane. At $x = 0$ and 0.12, the diffraction peak of $Mn_xFe_{3-x}O_4$ (004) nearly coincides with MgO (002). With the increase of Mn content, the $Mn_xFe_{3-x}O_4$ (004) peak separates from MgO (002) gradually due to the increasing lattice mismatch from 0.3% ($x = 0$) to 1.7% ($x = 0.65$). As shown in Fig. 1(b), the in-plane epitaxy of the typical $Mn_xFe_{3-x}O_4$ (001) films was verified by the φ scan of {111} reflections, demonstrating the epitaxial relationship $Mn_xFe_{3-x}O_4(001)\|MgO(001)$. Figure 1(c) displays Mn content dependent out-of-plane lattice constant c of the $Mn_xFe_{3-x}O_4$ films, where the lattice constant c increases slightly with the Mn content from 0.12 to 0.65. Given that the radii of Fe^{2+} (0.920 Å), Fe^{3+} (0.785 Å), Mn^{2+} (0.970 Å), and Mn^{3+} (0.785 Å), it is probable that Mn^{2+} exists in the $Mn_xFe_{3-x}O_4$ films. In order to obtain the chemical state of Mn directly, the peak of Mn $2p^{3/2}$ was found to be broadened at ~640 eV with X-ray photoelectron spectroscopy,[21,22] further indicating that chemical valence of Mn atoms is mainly +2 in the $Mn_xFe_{3-x}O_4$ films (not shown).

The location of Mn in the spinel ferrites is complicated.[23] Generally, in bulk, both normal spinel $Mn^{2+}(A)Fe^{3+}{}_2(B)O_4$ and inverse spinel $Fe^{3+}(A)Mn^{2+}(B)Fe^{3+}(B)O_4$ coexist in Mn ferrites.[18] It should be noted that normal spinel $Mn^{2+}(A)Fe^{3+}{}_2(B)O_4$ is an insulator due to the occupation of trivalent cations Fe^{3+} on B sites.[24] However, the reactively sputtered $Mn_xFe_{3-x}O_4$ films in this work is highly conductive, and the resistivity slightly increases from $\sim 10^4$ $\mu\Omega$ cm ($x = 0$) to $\sim 10^5$ $\mu\Omega$ cm ($x = 0.65$) by only one order of magnitude, which was also observed in other reports.[25] Furthermore, the free energy of $Mn_xFe_{3-x}O_4$ ($MnFe_{23}O_{32}$) with Mn occupied B sites is calculated to be ~0.3 eV smaller than that with Mn occupied A sites by DFT+U ($U_{Fe} = U_{Mn} = 4.5$ eV) technique. Hence Mn is prone to occupy B sites with +2 valence in the reactively sputtered $Mn_xFe_{3-x}O_4$ films.

The densities of states (DOS) of Fe_3O_4 and $Mn_5(B)Fe_{19}O_{32}$ ($x = 0.625$, close to the largest doping content $x = 0.65$ in the experiments) are given in Fig. 2, respectively. The states of minority spin located in the Fermi level in Fe_3O_4 are mainly from the 3d states of iron ions on B sites. Fortunately, besides the energy gap for majority spin getting smaller, the total densities of states near Fermi level were rarely affected by the B sites substitution of Mn for Fe, remaining the half-metallic band structure for the spin related applications. It thus can be understood that the double exchange among the iron ions on B sites is not destroyed completely for the relative smaller Mn incorporation ($x < 1$).

The morphology of the $Mn_xFe_{3-x}O_4$ films is displayed in the left column of Fig. 3. The surface is rather flat, with the roughness R_q slightly increasing from 0.128 Å ($x = 0.12$) to 0.842 Å ($x = 0.65$). The grain boundaries become more obvious with the increase of Mn content, and the grain size for the ~150 nm thick $Mn_{0.40}Fe_{2.60}O_4$ film in AFM images is ~80 nm, which is consistent with the estimated antiphase domain size.[26] The contrast of the MFM images, in the right column of Fig. 3, represents the antiferromagnetic coupled magnetic domains, where the size of magnetic domains increases with the increasing Mn content. The magnetic domain size of $Mn_xFe_{3-x}O_4$ films are ~120, ~165, and ~220 nm for $x = 0.12$, 0.40, and 0.65, respectively. Compared to the sample with $x = 0.12$, the $Mn_{0.65}Fe_{2.35}O_4$ film increases by ~80% in magnetic domain size. Since the density of APBs in Fe_3O_4 films is mainly decided by the film thickness and substrate temperature due to the diffusive motion,[26] it can be understood that the grain size nearly retains constant in the epitaxial $Mn_xFe_{3-x}O_4$ films due to the same film thickness and fabrication conditions. Therefore, by the incorporation of Mn atoms, the antiferromagnetic coupling across APBs is considered to be weakened, inducing the increase in magnetic domain size. Nevertheless, more explorations are needed to verify the reduction of antiferromagnetic coupling strength across APBs with the incorporation of Mn atoms.

And the Verwey transition temperature of the epitaxial Fe_3O_4 films in magnetization was determined to be ~95 K (Ref. 27), lower than ~125 K, which was probably caused by

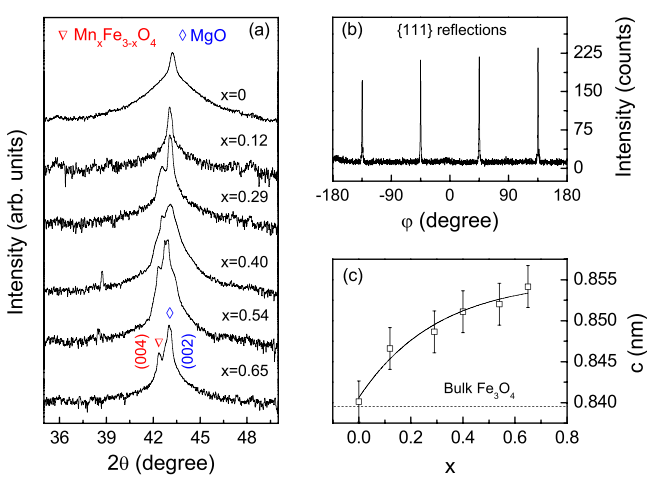

FIG. 1. (a) Enlarged X-ray diffraction θ-2θ patterns of the $Mn_xFe_{3-x}O_4$ films on MgO (001) near 43°, (b) typical in-plane φ scan of the $Mn_xFe_{3-x}O_4$ films with {111} reflections, (c) Mn content dependent out-of-plane lattice constant c, and the line is a guide to the eyes.

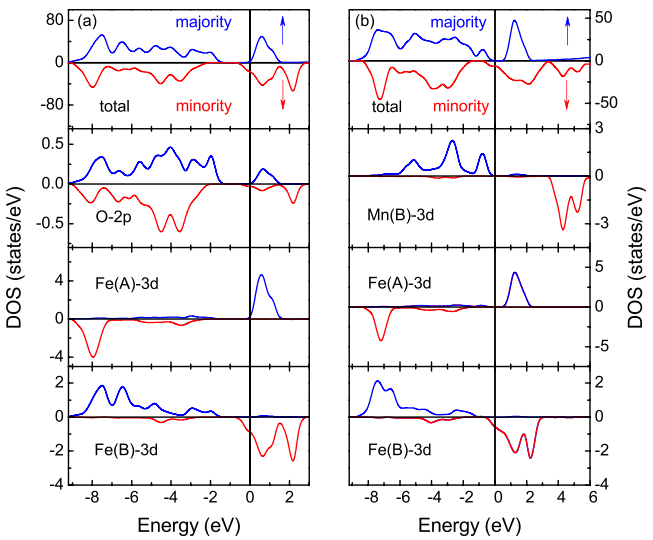

FIG. 2. Total and partial majority- and minority-spin DOS calculated with DFT+U for (a) $Fe_{24}O_{32}$ and (b) $Mn_5(B)Fe_{19}O_{32}$.

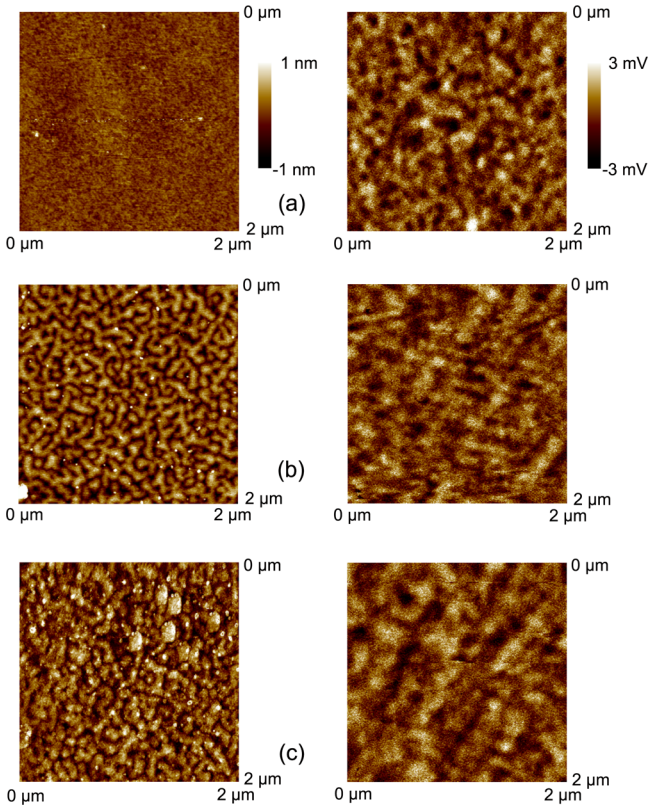

FIG. 3. Comparison of AFM (left column) and MFM (right column) images of the epitaxial $Mn_xFe_{3-x}O_4$ films, (a) $x = 0.12$, (b) $x = 0.40$, and (c) $x = 0.65$.

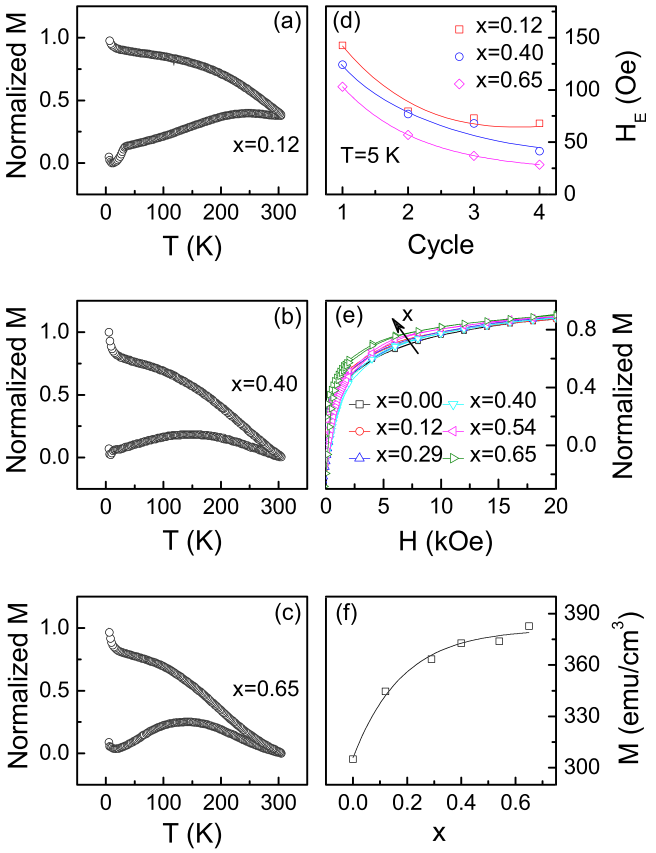

FIG. 4. Temperature dependence of ZFC and FC magnetization ($H = 500$ Oe) of the $Mn_xFe_{3-x}O_4$ films, (a) $x = 0.12$, (b) $x = 0.40$, and (c) $x = 0.65$. (d) Dependence of exchange bias on magnetic field cycle numbers with the cooling process from 300 K to 5 K at 70 kOe. (e) Normalized magnetization ($M/M_{70\ kOe}$) of the $Mn_xFe_{3-x}O_4$ films. (f) Dependence of saturation magnetization on Mn content. The solid lines in (d) and (f) are guide to the eyes.

the cation vacancy during the deposition. With the increase of number of cation vacancy on octahedral sites and interstitial cations Fe^{3+} on tetrahedral sites, entropy change at the Verwey transition decrease with the increasing δ in $Fe_{3(1-\delta)}O_4$. Verwey transition shifts from first-order transformation to second-order one, accompanied by the decrease of Verwey transition temperature.[28] As shown in Figs. 4(a)–4(c), with the increase of Mn content, Verwey transition disappears, further indicating the inclusion of Mn into the films. Attributed to the strong antiferromagnetic coupling between antiphase domains and nonlinear alignment of spin moments near APBs in the epitaxial Fe_3O_4 films, the temperature dependent zero field cooling (ZFC) and field cooling (FC) magnetizations always show significant branch at high temperatures.[27] The divergence of the ZFC and FC branches at high temperatures gets smaller with the increase of Mn content, which originates from the decrease of antiferromagnetic coupling strength between the antiphase domains. In order to directly observe the trend of antiferromagnetic coupling strength with Mn content, the exchange bias fields ($H_E = |H_{C+} - H_{C-}|/2$) of the $Mn_xFe_{3-x}O_4$ films were investigated through 70 kOe field cooling to 5 K. To train the exchange bias between the antiferromagnetic APBs and domains, the magnetic field cycled for four times. As displayed in Fig. 4(d), the exchange bias diminishes with the increase of the cycle number and Mn content, directly demonstrating the reduction of antiferromagnetic coupling strength with the increase of Mn content.

The normalized room temperature magnetizations ($M/M_{70\ kOe}$) of the epitaxial $Mn_xFe_{3-x}O_4$ films are given in Fig. 4(e) to show the low field magnetization behavior. Attributed to the weaker antiferromagnetic coupling strength across APBs, the low field magnetization saturates faster in the samples with higher Mn content, which was also observed in the epitaxial Fe_3O_4 films with different buffer layers reducing the density of APBs.[19] Figure 4(f) shows the dependence of room temperature saturation magnetization on Mn content. The magnetization slightly increases with Mn content from $\sim$310 emu/cm^3 ($x = 0.00$) to $\sim$380 emu/cm^3 ($x = 0.65$). The increase of magnetization is considered to be caused by the main substitution of Mn^{2+} (5 μ_B) for Fe^{2+} (4 μ_B) on B sites in the $Mn_xFe_{3-x}O_4$ films, inducing an increase of net moments between A and B sites. Compared to the saturation magnetization in bulk $\sim$480 emu/cm^3, the relatively lower saturation magnetization of the epitaxial Fe_3O_4 films in Fig. 4(f) is correlated with more occupation disorder including the partial cation vacancy (Fe^{2+} 4 μ_B or Fe^{3+} 5 μ_B) on B sites and interstitial cations Fe^{3+} on A sites.[28]

The magnetotransport properties of the Fe_3O_4 films are accepted to be dominated by the antiferromagnetic coupling across APBs. According to the spin-polarized transport across APBs, the magnetoresistance is expressed as[17]

$$MR \propto \frac{M_S H d^2}{J_{AF}^2 J_F^{-1}}, \quad (1)$$

where J_{AF} and J_F are the antiferromagnetic coupling strength across APBs and ferromagnetic coupling strength in the antiphase domains, respectively. M_S is the saturation magnetization and d the internal spin chain distance across APBs. As shown in Fig. 5(a), the linear field dependent magnetoresistance of the $Mn_xFe_{3-x}O_4$ films at 200 K slightly increases with the Mn content. Although spin chain distance d will increase correspondingly with the incorporation of Mn atoms, the MR ratio will be rarely affected by the slight increase of d because of the rather small lattice expansion in Fig. 1(c). Together with the saturation magnetization in Fig. 4(f), the relation of exchange interaction constant $J_{AF}^2 J_F^{-1}$ on Mn content x could be estimated from the MR value, as displayed in Fig. 5(b). The normalized exchange interaction constant $|J_{AF}^2 J_F^{-1}|$ decreases with the increasing Mn content. In order to understand the dependence of $|J_{AF}^2 J_F^{-1}|$ on x in Fig. 5(b), J_F and J_{AF} should be estimated individually.

To evaluate J_F in the antiphase domains directly, the interaction J_1 of $Fe^{2,3+}$(B)-O-Mn^{2+}(B) and antiferromagnetic exchange interaction J_2 of Fe^{3+}(A)-O-Mn^{2+}(B) were calculated according to the Heisenberg model

$$H = -2\sum_{i>j} J_{ij} S_i \cdot S_j, \tag{2}$$

where the quantum-mechanical Heisenberg Hamiltonian with $S = 5/2$ (Fe^{3+}, Mn^{2+}) or 2 (Fe^{2+}) was taken. The energy for the Mn_1(B)$Fe_{23}O_{32}$ with different magnetic configurations can be written as

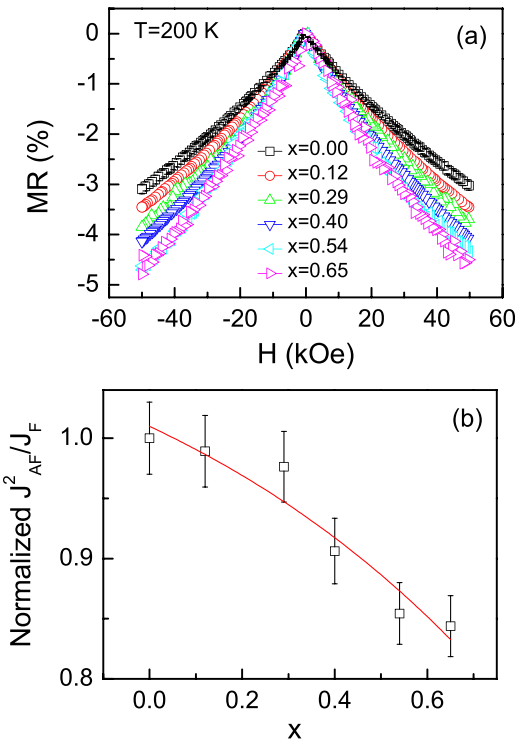

FIG. 5. (a) Magnetic field dependent magnetoresistance of the epitaxial $Mn_xFe_{3-x}O_4$ films at 200 K. (b) Mn content dependent normalized $|J_{AF}^2 J_F^{-1}|$ calculated by linear magnetoresistance according to Ref. 17, and the line is a guide to the eyes.

$$E_{AFM} = E_0 + 4.625 \times 2 \times \frac{5}{2} \times \frac{5}{2} \cdot J_2 + 6 \times \frac{5}{2} \times \left(\frac{5}{2} + 2\right) \cdot J_1, \tag{3a}$$

$$E_{FM} = E_0 - 4.625 \times 2 \times \frac{5}{2} \times \frac{5}{2} \cdot J_2 - 6 \times \frac{5}{2} \times \left(\frac{5}{2} + 2\right) \cdot J_1. \tag{3b}$$

Hence the calculated total energy difference ΔE can be expressed as

$$\Delta E_I = E_{AFM} - E_{FM} = 4.625 \times 4 \times \frac{5}{2} \times \frac{5}{2} \cdot J_2 + 6 \times 2 \times \frac{5}{2} \times \left(\frac{5}{2} + 2\right) \cdot J_1. \tag{4a}$$

B site substitution Mn for Fe with another Fe-O-Mn coordinate number was considered

$$\Delta E_{II} = E_{AFM} - E_{FM} = 4.5 \times 4 \times \frac{5}{2} \times \frac{5}{2} \cdot J_2 + 6 \times 2 \times \frac{5}{2} \times \left(\frac{5}{2} + 2\right) \cdot J_1. \tag{4b}$$

From Eqs. (4), J_1 and J_2 for Fe-O-Mn were calculated to be 8.62 and –15.46 meV, respectively. Similarly, the exchange J_1 and J_2 for Fe-O-Fe were obtained to be 37.78 and –41.55 meV, respectively.

It was found that J_1 for Fe-O-Mn among B sites is smaller than that of Fe-O-Fe, so the ferromagnetic coupling strength J_F ($\propto |J_1 - J_2|$) in antiphase domains for Mn doped Fe_3O_4 is smaller than that in Fe_3O_4 due to the additional double exchange interaction between Fe^{2+} and Fe^{3+}. Therefore, as displayed in Fig. 5(b), the decreasing normalized exchange interaction constant $|J_{AF}^2 J_F^{-1}|$ with the increase of Mn content should originate from the much faster reduction of J_{AF} across the APBs with the incorporation of Mn atoms.

While Mn was doped in the epitaxial Fe_3O_4 films, besides the superexchange interaction Fe-O-Fe, the interaction between Mn(B)-O-Mn(B) or Mn(B)-O-Fe(B) should also be taken into account to evaluate the antiferromagnetic coupling across APBs. Given that the larger ionic radius of Mn^{2+}(0.970 Å) than Fe^{2+} (0.920 Å) and Fe^{3+} (0.785 Å), the distance between Mn and O in the $Mn_xFe_{3-x}O_4$ films is larger than that between Fe and O in Fe_3O_4 films near APBs. Therefore, partial superexchange interaction J_{AF} Fe(B)-O-Mn(B) and Mn(B)-O-Mn(B) across APBs in the $Mn_xFe_{3-x}O_4$ films is weakened due to the larger Mn-O distance.

IV. CONCLUSION

In conclusion, the antiferromagnetic coupling strength J_{AF} across APBs in our highly conductive epitaxial Fe_3O_4 films was weakened by Mn incorporation, which was demonstrated by the larger magnetic domain size, faster saturated hysteresis loops, smaller exchange bias, and larger magnetoresistance. The decrease of J_{AF} with the increase of Mn content x is caused by the larger ionic radius of Mn^{2+} than those of

Fe^{2+} and Fe^{3+}. Meanwhile, it is proved that the 100% spin polarization near Fermi level can be maintained in the Mn doped Fe_3O_4. This result provides the way to pave the obstacle, strong antiferromagnetic coupling across APBs, for the applications of Fe_3O_4 films in spintronics.

ACKNOWLEDGMENTS

This work was supported by National Science Foundation of China (Grant No. 11204207), Ph.D. Programs Foundation of Ministry of Education of China (Grant No. 20120032120074), and Natural Science Foundation of Tianjin City (Grant No. 12JCYBJC11100).

[1]W. Döring, Ann. Phys. (Leipzig) **424**, 259 (1938).
[2]Y. S. Dedkov, U. Rüdiger, and G. Güntherodt, Phys. Rev. B **65**, 064417 (2002).
[3]M. Ziese, U. Kohler, A. Bollero, R. Hohne, and P. Esquinazi, Phys. Rev. B **71**, 180406R (2005).
[4]S. M. Watts, C. Boothman, S. V. Dijken, and J. M. D. Coey, Appl. Phys. Lett. **86**, 212108 (2005).
[5]G. Hu and Y. Suzuki, Phys. Rev. Lett. **89**, 276601 (2002).
[6]K. Ghosh, S. B. Ogale, S. P. Pai, M. Robson, E. Li, I. Jin, Z. W. Dong, R. L. Greene, R. Ramesh, and T. Venkatesan, Appl. Phys. Lett. **73**, 689 (1998).
[7]D. T. Margulies, F. T. Parker, F. E. Spada, R. S. Goldman, J. Li, R. Sinclair, and A. E. Berkowitz, Phys. Rev. B **53**, 9175 (1996).
[8]A. M. Bataille, L. Ponson, S. Gota, L. Barbier, D. Bonamy, M. G. Soyer, C. Gatel, and E. Snoeck, Phys. Rev. B **74**, 155438 (2006).
[9]H. Xiang, F. Y. Shi, M. S. Rzchowski, P. M. Voyles, and Y. A. Chang, Appl. Phys. Lett. **97**, 092508 (2010).
[10]F. C. Voogt, T. T. M. Palstra, L. Niesen, O. C. Rogojanu, M. A. James, and T. Hibma, Phys. Rev. B **57**, R8107 (1998).
[11]J. B. Moussy, S. Gota, A. Bataille, M. J. Guittet, M. G. Soyer, F. Delille, B. Dieny, F. Ott, T. D. Doan, P. Warin, P. B. Guillemaud, C. Gatel, and E. Snoeck, Phys. Rev. B **70**, 174448 (2004).
[12]T. Hibma, F. C. Voogt, L. Niesen, P. A. A. van der Heijden, W. J. M. de Jonge, J. J. T. M. Donkers, and P. J. van der Zaag, J. Appl. Phys. **85**, 5291 (1999).
[13]J. F. Bobo, D. Basso, E. Snoeck, C. Gatel, D. Hrabovsky, J. L. Gauffier, L. Ressier, R. Mamy, S. Visnovsky, J. Hamrle, J. Teillet, and A. R. Fert, Eur. Phys. J. B **24**, 43 (2001).
[14]S. Celotto, W. Eerenstein, and T. Hibma, Eur. Phys. J. B **36**, 271 (2003).
[15]G. A. Sawatzky, W. Geertsma, and C. Haas, J. Magn. Magn. Mater. **3**, 37 (1976).
[16]D. T. Margulies, F. T. Parker, M. L. Rudee, F. E. Spada, J. N. Chapman, P. R. Aitchison, and A. E. Berkowitz, Phys. Rev. Lett. **79**, 5162 (1997).
[17]W. Eerenstein, T. T. M. Plastra, S. S. Saxena, and T. Hibma, Phys. Rev. Lett. **88**, 247204 (2002).
[18]R. Arras, L. Calmels, and B. W. Fonrose, Phys. Rev. B **81**, 104422 (2010).
[19]C. Magen, E. Snoeck, U. Lüders, and J. F. Bobo, J. Appl. Phys. **104**, 013913 (2008).
[20]A. Kumar, D. K. Pandya, and S. Chaudhary, Appl. Phys. Lett. **102**, 152406 (2013).
[21]J. Gao, S. Y. Dai, and T. K. Li, Phys. Rev. B **67**, 153403 (2003).
[22]K. J. Kim, H. J. Lee, and J. Y. Park, J. Magn. Magn. Mater. **321**, 3706 (2009).
[23]J. P. Chen, C. M. Sorensen, K. J. Klabunde, G. C. Hadjipanayis, E. Devlin, and A. Kostikas, Phys. Rev. B **54**, 9288 (1996).
[24]V. N. Antonov, B. N. Harmon, and A. N. Yaresko, Phys. Rev. B **67**, 024417 (2003).
[25]M. Ishikawa, H. Tannka, and T. Kawai, Appl. Phys. Lett. **86**, 222504 (2005).
[26]W. Eerenstein, T. T. M. Palstra, T. Hibma, and S. Celotto, Phys. Rev. B **68**, 014428 (2003).
[27]P. Li, E. Y. Jiang, and H. L. Bai, J. Phys. D: Appl. Phys. **43**, 265002 (2010).
[28]J. P. Shepherd, J. W. Koenitzer, R. Aragon, J. Spalek, and J. M. Honig, Phys. Rev. B **43**, 8461 (1991).